

Training Symbol Based Coarse Timing Synchronization in OFDM Systems

Ming (Matt) Ruan, *Member, IEEE*, Mark C. Reed, *Senior Member, IEEE*, and Zhenning Shi, *Member, IEEE*

Abstract—In orthogonal frequency division multiplexing (OFDM) systems, coarse frame timing can be acquired from one or more training symbols preceding every OFDM burst. The existing literature studied the case where there was only one training symbol consisting of identical segments. We generalize the timing synchronization methods to take advantage of multiple training symbols and only require the segments to be highly correlated but not necessarily identical. We construct a series of component timing metrics, one for each pair of the highly correlated segments, and combine them linearly to minimize the false alarm probability while keeping the asymptotic missed detection probability to the same level as other techniques. The OFDM data symbols in a downlink burst can have different power levels to reach the users at different distances. We take that into account and yield more realistic results than those in existing literature which only considered the equal power case. The performance of the proposed method is analyzed in three scenarios generalized from the IEEE 802.11 and IEEE 802.16 standards. Numerical results are presented to confirm the robustness of the proposed method in various channel conditions.

Index Terms—Orthogonal frequency-division multiplexing (OFDM), synchronization.

I. INTRODUCTION

IN ORTHOGONAL frequency-division multiplexing (OFDM) systems, coarse timing synchronization is needed to indicate the start of a burst and determine the Fast Fourier Transform (FFT) window for each symbol in that burst. Schmidl and Cox [1] proposed to construct the training symbol with two identical halves in the time domain and estimate the beginning of OFDM symbols from the auto-correlation of the received signal. Coulson refined that algorithm in [2], and gave detailed performance analysis in [3]. Minn *et al.* [4] proposed to use a training symbol with more than two identical segments, and suggested to flip the signs of the segments with certain pattern to give the timing metric a steeper roll-off trajectory at the ideal timing position. Shi and Serpedin analyzed Minn's synchronization scheme in [5] and proposed a more advanced timing metric based on the maximum likelihood criterion.

The boundaries between the OFDM symbols are blurred by multipath wireless channels, so the ideal start of the FFT window at the receiver is usually difficult to locate in the

time domain. We know that, as long as the samples in the FFT window belong to the same OFDM symbol, the inter-symbol interference (ISI) and inter-carrier interference (ICI) are avoided. Therefore, it suffices for the coarse timing estimator to find an ISI-free FFT window of the training symbol. The residual timing offset results in a linear phase shift on the subcarriers, which can significantly degrade the performance of pilot-based channel estimation and tracking algorithms [6]. Then, the refined joint channel and timing estimators [7]–[9] are required for more accurate timing estimates using the frequency domain signal.

In some practical OFDM systems, like the IEEE 802.11 [10] and IEEE 802.16 [11], the training symbols are defined in the frequency domain by using one out of every M_i subcarriers, where i is the training symbol index. When M_i is not divisible by the number of subcarriers, e.g., $M_i = 3$ for the downlink of IEEE 802.16 OFDMA (WiMAX) systems, the training symbol is made up of highly correlated but not identical segments in the time domain. This scenario has not been investigated by the aforementioned literature, and only a heuristic solution is provided by Bhatt *et al.* [12].

This paper investigates the timing estimation methods based on the training symbols generalized from those specified by the standards [10], [11]. We propose to construct a series of component timing metrics, one for each pair of highly correlated segments in the training symbols. Then we linearly combine them to minimize the false alarm probability under the constraints on the correct detection performance. The component timing metrics only require the correlation between the segments to be high, so the proposed method is applicable to generalized training symbols including those specified by the IEEE 802.16 OFDMA (WiMAX) standard which have three highly correlated but not identical segments. Moreover, the proposed method takes advantage of multiple training symbols for further performance improvement. It is also worth noting that the data symbols in one OFDM burst can have different power levels to reach the users at different distances. We take that into account and yield more realistic results yet found in the existing literature.

The performance of the proposed method is analyzed in three scenarios generalized from the IEEE 802.11 and IEEE 802.16 standards. When there is one training symbol with two and four identical segments, the proposed method is equivalent to that in [1] and [5] respectively. Our analytical results show that using more identical segments in the training symbol only reduces false alarms and has little impact on the missed detection probability. This justifies our false alarm probability based optimization criterion, and contradicts the

Manuscript received March 13, 2008; revised June 14, 2008 and October 23, 2008; accepted January 11, 2009. The associate editor coordinating the review of this paper and approving it for publication was Dr. Justin Coon.

The authors are with the National ICT Australia and affiliated with the Australian National University. National ICT Australia is funded through the Australian Government's Backing Australia's Ability initiative and in part through the Australian Research Council. The authors can be contacted at {matt.ruan, mark.reed, zhenning.shi}@nicta.com.au.

existing timing metric design approach which is based on the detection probability. Simulations agree with our analytical results reasonably well and confirm the robustness of the proposed method in various channel conditions.

This paper is organized as follows. We define our system model in Section II, and then derive the proposed algorithm in Section III. The performance of the proposed method is analyzed in Section IV for three different scenarios generalized from the practical standards. Simulation results obtained with realistic channel models are presented in Section V and a brief summary concludes the paper in Section VI.

II. SYSTEM MODEL

We study packet oriented OFDM systems where one or more training symbols precede every OFDM burst to facilitate timing, frequency and channel estimation. The training symbols are defined in the frequency domain and only one out of every M_i subcarriers are used. More precisely, the time domain representation for the i^{th} training symbol reads

$$x_i(t) = (s(t) - s(t - (N + N_g)T_s)) \cdot \frac{1}{\sqrt{N}} \sum_{m=1}^{N_p[i]} X_i[m] e^{-j \frac{2\pi}{N} (\vartheta_i + (m-1)M_i) (\frac{t}{T_s} - N_g)} \quad (1)$$

where $s(t)$ is the unit step function which equals 1 when $t \geq 0$ and 0 otherwise; N is the number of subcarriers; T_s is $(1/N)$ -th of one symbol duration, which is also known as the sampling period; N_g is the length of the cyclic prefix (CP) in terms of samples. For the i^{th} training symbol, $N_p[i]$ is the number of used subcarriers, ϑ_i is the index of the first used subcarrier, $X_i[\cdot]$ is the phase shift keying (PSK) modulated pseudo-random training sequence mapped to the subcarriers $\{\vartheta_i, \vartheta_i + M_i, \dots, \vartheta_i + (N_p[i] - 1)M_i\}$. All the other subcarriers are not used. Using (1), for all $t \in [i(N + N_g)T_s, (i+1)(N + N_g)T_s - T_s N/M_i]$, we have

$$\begin{aligned} x_i(t + T_s N/M_i) &= \frac{1}{\sqrt{N}} \sum_{m=1}^{N_p[i]} X_i[m] \cdot e^{j \frac{2\pi}{N} (t/T_s + N/M_i - N_g) (\vartheta_i + (m-1)M_i)} \\ &= x_i(t) e^{j \frac{2\pi}{M_i} \vartheta_i}. \end{aligned} \quad (2)$$

This indicates that the time domain waveform of the training symbol is repeated every $(N/M_i)T_s$ with a fixed phase offset of $(2\pi\vartheta_i/M_i)$. Figure 1 shows an example of such generalized training symbols with $N = 8$ and $M_1 = 3$. The baseband signal $x_i(t)$ goes through the low-pass filter and is sampled at time interval T_s . We obtain a sequence of samples $x_i[n] = x_i(t)\delta(t - nT_s) = x_i(nT_s)$, where $\delta(\cdot)$ is the Dirac delta function. If N is not an integer multiple of M_i , the period of $x(t)$ is not equal to an integer number of samples, and the repetition structure is not preserved in the sample sequence $x[n]$. Figure 1 has illustrated this fact. The samples of the sine wave $x(t)$ are not periodical although the original waveform is.

After low-pass filtering and decimation, the baseband received signal can be represented as

$$r[n] = e^{j \frac{2\pi}{N} n \epsilon_0} (\hat{x}[n] + w[n]) \quad (3)$$

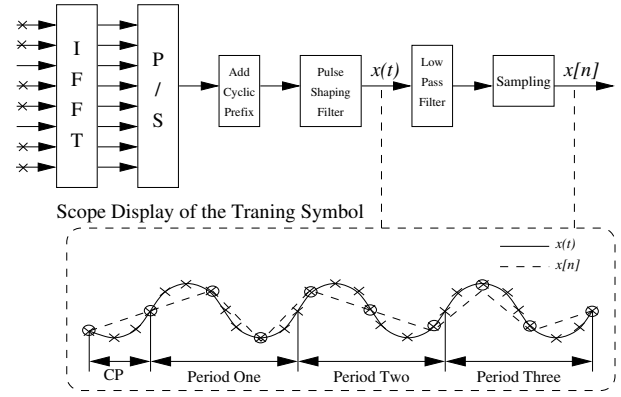


Fig. 1. Diagram of a generalized training symbol with $N = 8$, $M_1 = 3$.

where ϵ_0 is the true CFO normalized by the subcarrier spacing $1/(NT_s)$; I is the number of training symbols; $\tau[l]$ is the relative delay of the l^{th} channel tap, $h[l]$ is the complex representation of the tap's magnitude and phase; $w[n]$ is additive white Gaussian noise (AWGN) with variance σ_w^2 ; the fixed phase offset between the transmitter and receiver is absorbed in the channel coefficients, and we define $\hat{x}[n] \triangleq \sum_{l=1}^{L_h} h[l] \sum_{i=1}^I x_i[n - (i-1)(N + N_g) - \tau[l]]$. In this paper, the signal to noise ratio for the i^{th} training symbol is defined as the ratio between the signal and noise power in the received OFDM symbol: $\text{SNR}_i \triangleq (\sigma_i^2 / \sigma_w^2)$, where

$$\begin{aligned} \sigma_i^2 &\triangleq \frac{1}{N} \sum_{n=N_g}^{N+N_g-1} |\hat{x}[n + (i-1)(N + N_g)]|^2 \\ &= \frac{N_p[1]}{N} |X_i[1]|^2 \sum_{l=1}^{L_h} |h[l]|^2. \end{aligned} \quad (4)$$

The second equality of (4) follows Parseval's Theorem that the received signal's power in the time domain should equal that in the frequency domain. It should be noted that the received signal within the CP may come from two OFDM symbols in a multipath channel, so we exclude it from the signal power calculation.

III. THE METHOD

In the time domain, the high autocorrelation between the segments of the training symbol distinguishes the preamble from the noise and other OFDM symbols in the burst. This means that timing can be estimated from any pair of correlated segments. When multiple pairs exist in one or multiple training symbols, one would intuitively want to combine them for enhanced performance. In this section, we first analyze the statistical properties of the correlators and component timing metrics, then derive the coefficients to combine them in a linear manner such that the false alarm probability is minimized under the constraints on missed detection performance. A brief summary concludes the section.

A. Correlators

Since the high autocorrelation distinguishes the training symbol from others, we follow the traditional works [1]–[5]

and base our timing estimator on the correlators defined as

$$R[n, d] \triangleq \sum_{k=0}^{N-d-1} r^*[n+k]r[n+k+d] \quad (5)$$

where $(\cdot)^*$ denotes complex conjugate. The correlator given by (5) can be easily implemented on hardware using the integrate-and-dump algorithm [3].

Denote \hat{n}_i as the ideal start of the FFT window at the receiver for the i^{th} training symbol. In Appendix A, we show that when the signal is stronger than the noise and d is close to a multiple of N/M_i ,

$$R[\hat{n}_i, d] \approx e^{j\frac{2\pi}{N}\epsilon_0 d} ((N-d)\sigma_i^2 \phi_i(d) \rho_i(d) + \Theta(\hat{n}_i, d)) \quad (6)$$

where

$$\begin{aligned} \Theta(\hat{n}_i, d) \triangleq & \sum_{k=0}^{N-d-1} w^*[\hat{n}_i+k]\hat{x}[\hat{n}_i+k+d] \\ & + \sum_{k=d}^{N-1} w[\hat{n}_i+k]\hat{x}^*[\hat{n}_i+k-d] \end{aligned} \quad (7)$$

and

$$\rho_i(d) \triangleq \begin{cases} 1, & d \text{ is multiple of } (N/M_i); \\ \frac{\sin(\frac{\pi}{N}M_i d N_p[i])}{N_p[i] \sin(\frac{\pi}{N}M_i d)}, & \text{others.} \end{cases} \quad (8)$$

$$\phi_i(d) \triangleq \begin{cases} e^{j\frac{2\pi}{N}\theta_i d}, & d \text{ is multiple of } (N/M_i); \\ e^{j\frac{\pi d (M_i(N_p[i]-1)+2\theta_i)}{N}}, & \text{others.} \end{cases} \quad (9)$$

We can see that only the first term in the bracket of the right hand side of (6) represents the useful signal, whose magnitude is given by $(N-d)|\rho_i(d)|$. Because $|\rho_i(d)|$ decays quickly as d moves away from a multiple of N/M_i , we propose to choose

$$d_{i,k} \triangleq [k N/M_i], \quad (10)$$

where $k \in [1, M_i-1]$, and $[\cdot]$ denotes the function that outputs the integer closest to its argument. The existing papers [1]–[5] have only studied the case where N/M_i is an integer, while this paper investigates a more general scenario that covers the generic WiMAX training symbols where $M_i = 3$. It is worth noting that when $d = 0$, $E\{R[\hat{n}_i, 0]\} = N(\sigma_i^2 + \sigma_w^2)$ gives the signal plus noise energy.

B. Component Timing Metrics

A timing metric measures the likelihood of a given timing position to be the start of a training symbol. We know that the correlators can detect the highly correlated segments in a training symbol, so each one of them can be a timing metric. However, as revealed by (6), the output of a correlator fluctuates with the received signal strength. To avoid the adverse impact of power fluctuation, we normalize the correlator so that at the ideal timing position \hat{n}_i the expectation of the correlation equals 1. Ideally, the normalization can be performed as

$$\frac{|R[\hat{n}_i, d_{i,k}]|}{E\{|R[\hat{n}_i, d_{i,k}]\}} = \frac{N}{N-d_{i,k}} \cdot \frac{1}{|\rho_i(d_{i,k})|} \cdot \frac{|R[\hat{n}_i, d_{i,k}]|}{N\sigma_i^2}. \quad (11)$$

Because the knowledge of signal power σ_i^2 is not available to the receiver, the ideal normalization is not practical. An approximation to that is to use $R[\hat{n}_i, 0]$ as an estimate of $N\sigma_i^2$, and we define the component timing metric as

$$T_c[n, d_{i,k}] \triangleq \frac{N}{N-d_{i,k}} \cdot \frac{1}{|\rho_i(d_{i,k})|} \cdot \frac{|R[n, d_{i,k}]|}{R[n, 0]}. \quad (12)$$

At perfect timing position \hat{n}_i , using (6), we have

$$\begin{aligned} T_c[\hat{n}_i, d] &= \frac{N}{N-d} \frac{1}{|\rho_i(d)|} \cdot \frac{|R[\hat{n}_i, d]|}{R[\hat{n}_i, 0]} \\ &\approx \frac{N}{N-d} \frac{1}{|\rho_i(d)|} \cdot \frac{(N-d)|\rho_i(d)|\sigma_i^2}{N(\sigma_i^2 + \sigma_w^2)} \\ &= \frac{\sigma_i^2}{\sigma_i^2 + \sigma_w^2}. \end{aligned} \quad (13)$$

This indicates that at high SNR the timing metric is very close to 1. We also note that the timing metrics in the references [1], [2], [4] are equivalent to the component timing metric $T_c[n, (N/M_i)]$ when M_i is divisible by N .

Denote \bar{n}_i as a timing position that is far away from the ideal one \hat{n}_i , i.e., none of the samples from \bar{n}_i to $\bar{n}_i + N - 1$ belong to the i^{th} training symbol. In Appendix B, we show that in AWGN channels and for both equal and unequal power cases, $T_c[\bar{n}_i, d_{i,k}]$ can be well approximated by a Rayleigh distributed random variable with cumulative distribution function (cdf)

$$P(T_c[\bar{n}_i, d_{i,k}] < \lambda) \approx \int_0^\lambda f(x|\bar{\sigma}_{i,k}^2) dx = 1 - e^{-\frac{\lambda^2}{2\bar{\sigma}_{i,k}^2}} \quad (14)$$

where $f(x|\bar{\sigma}_{i,k}^2) = \frac{x}{\bar{\sigma}_{i,k}^2} e^{-\frac{x^2}{2\bar{\sigma}_{i,k}^2}}$ and $\bar{\sigma}_{i,k}^2 = \frac{1}{2} \frac{1}{\rho_i^2(d_{i,k})} \frac{1}{N-d_{i,k}}$. Our simulation shows that, in multipath channels where the channel delay spread is much shorter than the OFDM symbol duration, (14) is also a good approximation to the true statistics of the component timing metric.

C. Combining the Timing Metrics

Multiple component timing metrics can be constructed for the training symbols. Although each one of them gives a timing estimate, it is possible to combine them for better performance. We propose to linearly combine the component timing metrics to minimize the false alarm probability while keeping the asymptotic missed detection probability low. The combined timing metric is defined as

$$T[n] \triangleq \sum_{i=1}^I \sum_{k=1}^{K_i} \omega_{i,k} T_c[n + (i-1)(N+N_g), d_{i,k}] \quad (15)$$

where $K_i = M_i - 1$ is the number of component metrics constructed for training symbol i , and $\{\omega_{i,k}\}$ are the coefficients that need to be determined according to two criteria:

- In a noiseless channel, at the ideal timing position \hat{n}_1 , $T[\hat{n}_1] \approx 1$.
- At a wrong timing position \bar{n}_1 , the probability for $T[\bar{n}_1]$ to reach the given threshold λ should be minimized.

To meet the first criterion, from (13) and (15), it requires that

$$\sum_{i=1}^I \sum_{k=1}^{K_i} \omega_{i,k} = 1. \quad (16)$$

Under this constraint, we compute the coefficients $\{\omega_{i,k}\}$ satisfying the second criterion as follows.

At a wrong timing position \hat{n}_1 , a false alarm occurs if the combined timing metric reaches the threshold λ . As shown in Appendix C, the false alarm probability is given by

$$P(T[\hat{n}] \geq \lambda) \approx (\sqrt{2\pi})^{K-1} \lambda^{K-1} e^{-\frac{\lambda^2}{2 \sum_{i=1}^I \sum_{k=1}^{K_i} \omega_{i,k}^2 \bar{\sigma}_{i,k}^2}} \cdot \frac{\sqrt{\prod_{i=1}^I \prod_{k=1}^{K_i} \omega_{i,k}^2 \bar{\sigma}_{i,k}^2}}{\left(\sum_{i=1}^I \sum_{k=1}^{K_i} \omega_{i,k}^2 \bar{\sigma}_{i,k}^2\right)^{K-\frac{1}{2}}} \quad (17)$$

where $K = \sum_{i=1}^I K_i$. For high thresholds, the false alarm probability is determined by the denominator of the exponent

$$\varpi \triangleq \sum_{i=1}^I \sum_{k=1}^{K_i} \omega_{i,k}^2 \bar{\sigma}_{i,k}^2. \quad (18)$$

Under the constraint in (16), we can show the coefficients $\{\omega_{i,k}\}$ that minimize ϖ are given by

$$\omega_{i,k} = \frac{\rho_i^2(d_{i,k})(N - d_{i,k})}{\sum_{i=1}^I \sum_{m=1}^{K_i} \rho_i^2(d_{i,m})(N - d_{i,m})}. \quad (19)$$

And, it follows that

$$\varpi = \frac{1}{\sum_{i=1}^I \sum_{n=1}^{K_i} \rho_i^2(d_{i,n})(N - d_{i,n})}. \quad (20)$$

This means that the component metrics must have large $|\rho_i(d_{i,k})|$ values to make significant contribution to the combined timing metric. This justifies our selection of $\{d_{i,k}\}$ in (10).

D. Summary

We briefly summarize the proposed coarse timing estimator as follows.

- 1) Construct $(M_i - 1)$ component timing metrics $T_c[n, d_{i,k}]$ for each training symbol using (12) where $\{d_{i,k}\}$ are given by (10).
- 2) Compute the combined timing metric $T[n]$ using (15) where $\{\omega_{i,k}\}$ are given by (19).
- 3) Once the combined timing metric $T[n]$ reaches the detection threshold λ , the position corresponding to the maximum of the timing metric within the following N OFDM samples is the coarse timing estimate.

It should be noted that choosing the maximum of the timing metric within certain window avoids the dependency of coarse timing estimates on the threshold setting. Shi and Serpedin [5] assumed the coarse timing estimate to be where the threshold is first reached. Figure 2 shows an example to illustrate the difference between their approach and ours. It is shown that our estimates are independent of the threshold settings and must fall in the correct timing window for any threshold lower than the peak. However, Shi and Serpedin's estimates are determined by the threshold settings, which have to be precisely set close to the peak to obtain correct estimates. In practical OFDM systems where the timing metrics change dramatically from burst to burst due to the channel variation, our approach gives more robust performance.

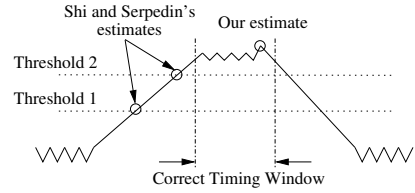


Fig. 2. Comparison of coarse timing estimates from a typical timing metric.

IV. PERFORMANCE ANALYSIS AND CASE STUDY

To provide more insights into the proposed algorithm, we analyze the performance in three special cases generalized from the IEEE 802.11 [10] and IEEE 802.16 [11] standards. In Case A, we compare our estimator to those conventional methods [1], [5] and shed new light on them; in Case B, we investigate the gain of combining the second training symbol into the timing metric; in Case C, we analyze the performance of the proposed method for generic WiMAX training symbols.

A. Case A: One training symbol, N is multiple of M_1

This case generalizes the uplink training symbol in IEEE 802.16 [11] OFDM systems where the data OFDM symbols are placed after the training symbol which is QPSK modulated and $M_1 = 4$. From (19), we can compute

$$\omega_{1,k} = \frac{(N - kN/M_1)}{\sum_{m=1}^{M_1-1} (N - mN/M_1)} = \frac{2(M_1 - k)}{M_1(M_1 - 1)}. \quad (21)$$

The combined timing metric becomes

$$T[n] = \frac{2}{M_1 - 1} \frac{\sum_{i=1}^{M_1-1} \left| \sum_{k=0}^{N-i/M_1} r^*[n+k]r[n+k+i/M_1] \right|}{\sum_{k=0}^{N-1} |r[n+k]|^2}. \quad (22)$$

Although derived from different optimization criteria, the proposed timing metric coincides with those in [1], [5] respectively for $M_1 = 2$ and $M_1 = 4$ cases. It is easy to compute

$$\varpi = \sum_{k=1}^{M_1-1} \omega_{1,k}^2 \bar{\sigma}_{1,k}^2 = \frac{2}{N(M_1 - 1)}. \quad (23)$$

This indicates that the false alarm probability decreases as the number of identical segments increases.

Next, we analyze the missed detection probability. Define

$$Z_A[\hat{n}_1] \triangleq R_A[\hat{n}_1] - \lambda R[\hat{n}_1, 0] \quad (24)$$

where $R_A[\hat{n}_1] \triangleq \frac{2}{M_1-1} \sum_{k=1}^{M_1-1} |R[\hat{n}_1, d_{1,k}]|$. As shown in Appendix D,

$$E\{Z_A[\hat{n}_1]\} = N\sigma_1^2(1 - \lambda) - N\sigma_w^2\lambda \quad (25)$$

$$\text{Var}\{Z_A[\hat{n}_1]\} \approx 2N\sigma_1^2\sigma_w^2(1 - \lambda)^2. \quad (26)$$

Following [3] and [5], we approximate $Z_A[\hat{n}_1]$ by a Gaussian random variable, and the missed detection probability is given by

$$P(T[\hat{n}_1] < \lambda) = P(Z_A[\hat{n}_1] < 0) \approx \frac{1}{2} \text{erfc} \left(\frac{\sqrt{N}}{2} \left(\sqrt{\frac{\sigma_1^2}{\sigma_w^2}} - \frac{\lambda}{1 - \lambda} \sqrt{\frac{\sigma_w^2}{\sigma_1^2}} \right) \right) \quad (27)$$

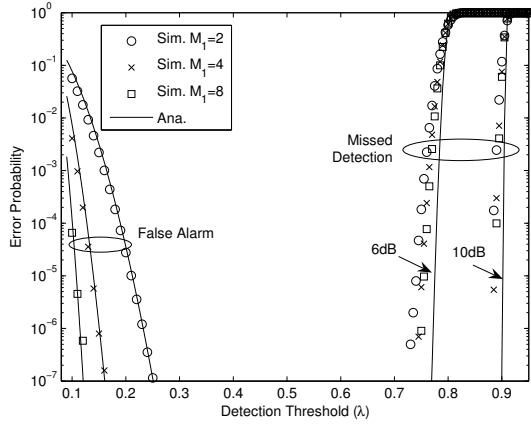


Fig. 3. Performance in AWGN channel (Case A).

where $\text{erfc}(z) \triangleq \frac{2}{\sqrt{\pi}} \int_z^{+\infty} e^{-t^2} dt$. This indicates that the missed detection probability monotonously decreases to zero as the SNR (σ_1^2/σ_w^2) increases. And, to limit the missed detection probability within 50%, it requires $\lambda \leq \frac{\sigma_1^2}{\sigma_w^2 + \sigma_1^2}$. This upper bound of λ varies from 0.5 to 0.9 as the SNR increases from 0dB to 10dB, which indicates that the missed detection probability is highly sensitive to the noise level, and optimizing the threshold for a large range of SNR is virtually impossible. Another interesting observation from (27) is that the missed-detection probability does not depend on M_1 . This means that using more identical segments in the training symbol will not lower the missed detection probability. In other words, Schmid's estimator [1] cannot be outperformed in terms of missed detection probability by more complex algorithms including Shi and Serpedin's method [5].

We numerically evaluate the missed detection and false alarm probabilities of Case A for an unequal power OFDM system with 512 subcarriers in an AWGN channel. 5% of the subcarriers at each end of the spectrum are unused, and the CFO is modeled by a random variable uniformly distributed in $[-10, 10]$ subcarrier spacing. When testing the false alarm probability, the relative power level of each OFDM symbol is independently selected from $\{-12\text{dB}, -9\text{dB}, \dots, +9\text{dB}\}$ with equal probability and the noise power is fixed to -10dB . The modulation scheme for each data symbol is independently selected from QPSK, 16-QAM or 64-QAM also with equal probability. When testing the missed detection probability, the training symbol is QPSK modulated and randomly generated for each experiment, and we change the power of the training symbol to validate our analytical results. In Figure 3, the solid lines represent the analytical results given by (17) and (27), and the various markers represent the simulation results averaged for at least 10^5 independent OFDM symbols. The figure shows that our analysis matches the simulation results very well.

B. Case B: Two training symbols, N is multiple of both M_1 and M_2

This case generalizes the short and long training symbol schemes specified in the IEEE 802.11 and IEEE 802.16

standards. In the former, $N = 128$, $M_1 = 8$, $M_2 = 2$; in the latter, $N = 256$, $M_1 = 4$, $M_2 = 2$. From (19), we can calculate

$$\begin{aligned} \omega_{i,k} &= \frac{N - kN/M_i}{\sum_{i=1}^{M_1-1} (N - iN/M_1) + \sum_{i=1}^{M_2-1} (N - iN/M_2)} \\ &= \frac{2(M_i - k)}{M_i(M_1 + M_2 - 2)}. \end{aligned} \quad (28)$$

The false alarm probability decays exponentially with the inverse of

$$\varpi = \sum_{i=1}^2 \sum_{k=1}^{M_i-1} \omega_{i,k}^2 \bar{\sigma}_{i,k}^2 = \frac{2}{N} \frac{1}{M_1 + M_2 - 2}. \quad (29)$$

Comparing (29) to that of Case A in (23), we can see the benefit of combining the long preamble is negligible when the number of identical segments in the short training symbol is large, i.e., in the IEEE 802.11 case. However, for smaller M_1 as in the IEEE 802.16 case, the combined metric gives much fewer false alarms.

Similar to the approach we used in Case A, define

$$\begin{aligned} Z_B[\hat{n}_1] &\triangleq R_{B,1}[\hat{n}_1]R[\hat{n}_2, 0] + R_{B,2}[\hat{n}_2]R[\hat{n}_1, 0] \\ &\quad - \lambda R[\hat{n}_1, 0]R[\hat{n}_2, 0] \end{aligned} \quad (30)$$

where $R_{B,i}[\hat{n}_i] \triangleq \frac{2}{M_1 + M_2 - 2} \sum_{k=1}^{M_i-1} |R[\hat{n}_i, d_{i,k}]|$. In Appendix E, we show that

$$E\{Z_B[\hat{n}_1]\} = N^2 \sigma_1^2 (\sigma_1^2 + \sigma_w^2) - \lambda N^2 (\sigma_1^2 + \sigma_w^2)^2 \quad (31)$$

$$\text{Var}\{Z_B[\hat{n}_1]\} \approx 4N^3 \sigma_1^6 \sigma_w^2 (1 - \lambda)^2. \quad (32)$$

Thus,

$$\begin{aligned} P(T[\hat{n}_1] < \lambda) &= P(Z_B[\hat{n}_1] < 0) \\ &\approx \frac{1}{2} \text{erfc} \left(\frac{\sqrt{N}}{2\sqrt{2}} \left(\sqrt{\frac{\sigma_1^2}{\sigma_w^2}} - \frac{\lambda}{1 - \lambda} \sqrt{\frac{\sigma_w^2}{\sigma_1^2}} \right) \right). \end{aligned} \quad (33)$$

Compared to (27),

- The 50% missed detection probability corresponds to $\lambda = \sigma_1^2/(\sigma_1^2 + \sigma_w^2)$, which is same as that of Case A.
- Combining the timing metric of the second symbol slightly increases the missed detections at high SNR.
- Because the missed detection probability given by (33) is not a function of M_1 or M_2 , using more identical segments in the training symbols does not reduce missed detections.

We verify the analytical results using the same simulation environment as that of Case A and plot the results in Figure 4. The analytical and simulation results for Case B are represented by the solid lines and the various markers respectively. The dotted lines are the analytical results in the scenario where only the short training symbol is utilized. It is shown that our analysis agrees with the simulations reasonably well. The figure suggests that using both training symbols can considerably reduce the false alarm probability for the $M_1 = 4$ case, but the improvement is marginal for the $M_1 = 8$ case. The missed detection curves of Case A and B are very close to each other under the given SNRs, and all of them exhibit very steep rising edges. This means that combining

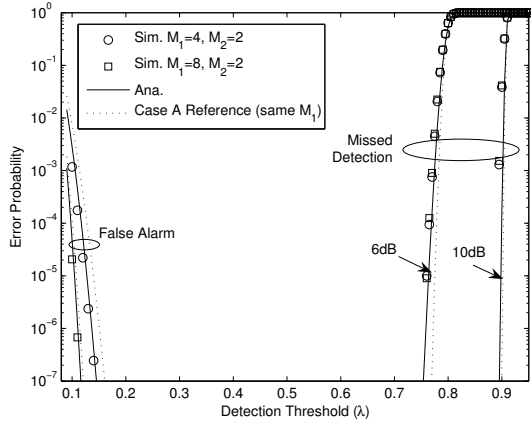


Fig. 4. Performance in AWGN channel (Case B).

two training symbols does not have practical impact on the detection performance, which is largely determined by the SNR.

C. Case C: One training symbol, N is not multiple of M_1

This case generalizes the IEEE 802.16 OFDMA (WiMAX) downlink channel where $M_1 = 3$. In this case,

$$\begin{aligned} \omega_{1,k} &= \frac{(N - d_{1,k})\rho_1^2(d_{1,k})}{\sum_{m=1}^{M_1-1} \rho_1^2(d_{1,m})(N - d_{1,m})} \\ &= \frac{2(N - d_{1,k})}{N} \frac{\rho_1^2(d_{1,k})}{\sum_{m=1}^{M_1-1} \rho_1^2(d_{1,m})} \end{aligned} \quad (34)$$

where the last equality follows the fact that $|\rho_i(d)| = |\rho_i(N - d)|$. The combined metric's false alarm probability is determined by

$$\varpi = \sum_{k=1}^{M_1-1} \omega_{1,k}^2 \bar{\sigma}_{1,k}^2 = \frac{2}{N} \frac{1}{\sum_{k=1}^{M_1-1} \rho_1^2(d_{1,k})}. \quad (35)$$

Define

$$Z_C[\hat{n}_1] \triangleq R_C[\hat{n}_1] - \lambda R[\hat{n}_1, 0] \quad (36)$$

where $R_C[\hat{n}_1] \triangleq \frac{2}{\sum_{k=1}^{M_1-1} \rho_1^2(d_{1,k})} \sum_{k=1}^{K_1} |\rho_1(d_{1,k})R[\hat{n}_1, d_{1,k}]|$. In Appendix D, we show that

$$E\{Z_C[\hat{n}_1]\} = N\sigma_1^2 - N\lambda(\sigma_1^2 + \sigma_w^2) \quad (37)$$

and

$$\begin{aligned} \text{Var}\{Z_C[\hat{n}_1]\} &\approx 2\lambda^2 N\sigma_1^2\sigma_w^2 - 4\lambda N\sigma_1^2\sigma_w^2 \\ &+ \left(\frac{2}{\sum_{k=1}^{M_1-1} |\rho(d_{1,k})|^2}\right)^2 \sum_{k_1=1}^{M_1-1} \sum_{k_2=1}^{M_1-1} \rho(d_{1,k_1})\rho(d_{1,k_2}) \\ &\cdot ((N - \max(d_{1,k_1}, d_{1,k_2}))\rho(d_{1,k_2} - d_{1,k_1}) \\ &+ \max(N - d_{1,k_1} - d_{1,k_2}, 0)\rho(d_{1,k_2} + d_{1,k_1})). \end{aligned} \quad (38)$$

From (37), we can tell that the threshold corresponding to 50% missed detection probability of Case C is the same as those of Case A and B. Considering the steepness of the missed detection curves, we expect the detection performance of Case C to be similar to that in the former two cases.

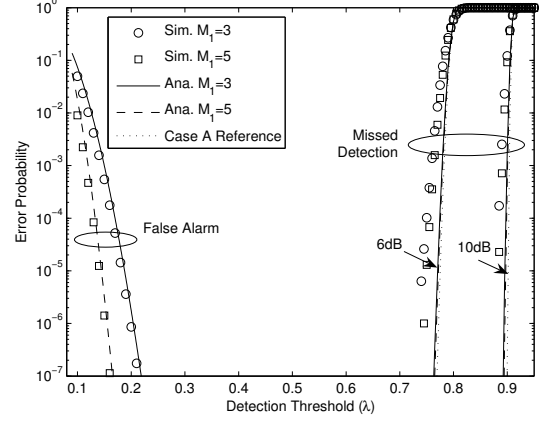


Fig. 5. Performance in AWGN channel (Case C).

We verify the analytical results using the same simulation environment as that of Case A. The results are plotted in Figure 5 where we use solid and dashed lines to represent the analytical results, and various markers to represent the simulation results. Also, we use dotted lines to represent the analytical missed detection probabilities of Case A under the given SNRs. It is shown that our analysis agrees with the simulations reasonably well. The figure suggests that using more highly correlated segments in the training symbols reduces false alarms but has little impact on the missed detection probability, which is largely determined by the SNR. These results coincide with our findings in the former two cases.

V. SIMULATION RESULTS

In this section, we present simulation results in realistic wireless communication scenarios. An IEEE 802.16 [11] (WiMAX) system is modeled in the simulations using two kinds of training symbols specified for the OFDM and OFDMA physical layers respectively. The OFDM physical layer has $N = 256$ subcarriers, and employs two training symbols with $M_1 = 4$ and $M_2 = 2$. The OFDMA physical layer has $N = 512$ subcarriers and uses only one training symbol with $M_1 = 3$. The carrier frequency is set to 3.5GHz, cyclic prefix is 1/8 of one symbol duration. The true CFO is modeled by a uniformly distributed random variable within ± 20 subcarrier spacing. Each OFDM burst lasts for 5ms, containing 47 OFDM symbols plus an idle period between the bursts. Every point in the figures is an average of at least 3×10^4 independent experiments, each of which contains at least one complete OFDM burst, but the starting position of observation is randomly selected. The training symbols have equal power, which is 9dB higher than the average power level of data symbols. Each data symbol's relative power level is independently selected from $\{-12\text{dB}, -9\text{dB}, \dots, +9\text{dB}\}$ with equal probability, and the modulation scheme is randomly selected from QPSK, 16-QAM or 64-QAM also with equal probability. The SNR is defined as the ratio between the average power of the signal and noise in every received OFDM sample of the training symbol.

Two channel models are used in the simulations, namely “CH-A” and “CH-B”. CH-A is a stationary wireless communication channel known as SUI-3 [13]. The channel has 3 taps with relative delays $\{0, 0.4\mu\text{s}, 0.9\mu\text{s}\}$ and power $\{0\text{dB}, -5\text{dB}, -10\text{dB}\}$. The magnitude of the first channel tap follows Rice distribution, and those of the other two are Rayleigh distributed. CH-B follows the power delay profile of the Vehicular-A channel in [14], which has 6 taps with relative delays $\{0, 0.31\mu\text{s}, 0.71\mu\text{s}, 1.09\mu\text{s}, 1.73\mu\text{s}, 2.51\mu\text{s}\}$ and power $\{0\text{dB}, -1\text{dB}, -9\text{dB}, -10\text{dB}, -15\text{dB}, -20\text{dB}\}$. The Doppler frequency of CH-A is only 0.4Hz, so within each OFDM symbol, the channel almost remains the same. We use Jakes’ model [15] to emulate the Rayleigh fading on each tap of CH-B where the vehicle speed is set to 120km/h and the maximum Doppler frequency is given by

$$f_d = \frac{120\text{km/h} \cdot 3.5 \times 10^9\text{Hz}}{3 \times 10^8\text{m/s}} \approx 388.9\text{Hz}. \quad (39)$$

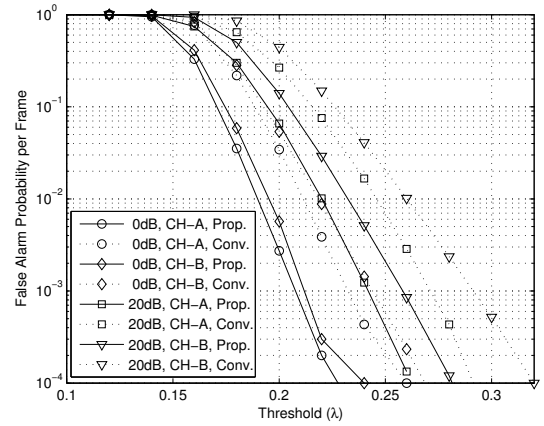
In the simulations, each OFDM symbol lasts for $91\mu\text{s}$, which gives $Nf_dT_s = 0.0354$. We move the channel taps to the nearest sample-spaced position to simplify the channel emulation.

In the simulations, we take the maximum of the timing metric within the window $[\hat{n}_i - N, \hat{n}_i + N]$ as the timing estimate. As we explained earlier, our coarse timing estimates do not depend on the threshold settings, and for all the thresholds that allow the detection of the OFDM burst, the timing estimates will be the same.

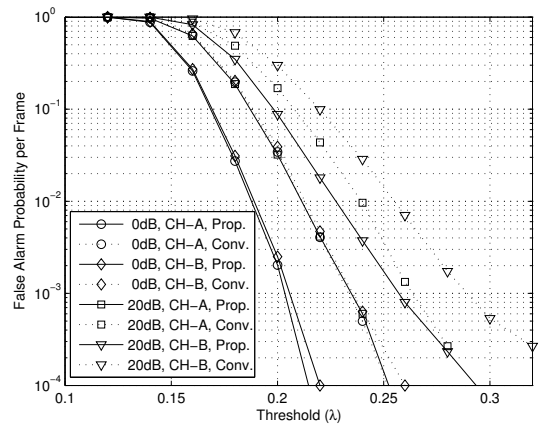
For the OFDM physical layer, we refer to the method of [5] as the conventional method, which only uses the short training symbol for timing estimation. In Figure 6(a), 7(a) and 8(a), we compare that to the proposed method which can take advantage of multiple training symbols. For the OFDMA physical layer, we refer to the method of [12] as the conventional method, which only uses the first component timing metric for timing estimation. In Figure 6(b), 7(b) and 8(b), we compare that to the proposed method which employs two timing metrics combined for lower false alarm rate. In both OFDM and OFDMA cases, the proposed methods require one more component timing metric than the conventional methods.

A. False Alarm Probability

Figure 6(a) and 6(b) show the false alarm probabilities as a function of the threshold λ for OFDM and OFDMA physical layers respectively. It is shown that the proposed method achieves much better performance than the conventional methods [5], [12] in all the cases. The false alarm probability at 0dB is lower than that at 20dB. This can be explained by the fact that higher SNR causes larger power variation within one OFDM symbol, which violates our assumptions when deriving the variance of the component timing metrics in Appendix B. For the same reason, the time-selectivity in CH-B degrades the performance of the combined timing metric. However, the figure shows that the conventional methods also suffer from the power fluctuation, and the advantage of the proposed method in terms of missed detection performance is quite evident.



(a) OFDM physical layer ($M_1 = 4, M_2 = 2$)



(b) OFDMA physical layer ($L_1 = 3$)

Fig. 6. False alarm probability per frame.

B. Missed Detection Probability

The missed detection probabilities are plotted in Figure 7(a) and 7(b) respectively for OFDM and OFDMA physical layers. The figures show that virtually no difference between the missed detection performance of the proposed method and that of the conventional methods [5], [12]. However, the curves of different SNRs differ dramatically with each other. This confirms our analytical results that the missed detection probability is highly sensitive to SNR, which fluctuates with the channel condition in a wide range. Therefore, optimizing the detection performance at certain SNR cannot give a timing metric with stable performance in various channel conditions. Nevertheless, for any given false alarm probability, our method allows the use of a lower threshold, which gives a better chance to detect the right timing position.

C. Distribution of Timing Offsets

As explained in the introduction, we define the correct timing positions to be those that incur little or no ISI in the FFT windows. We take the middle point of CP as the reference timing position, and compute the probability for the

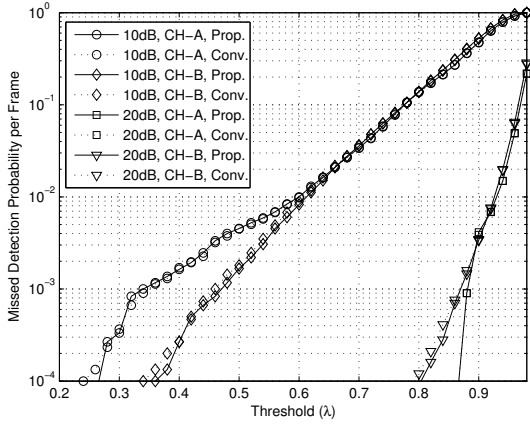
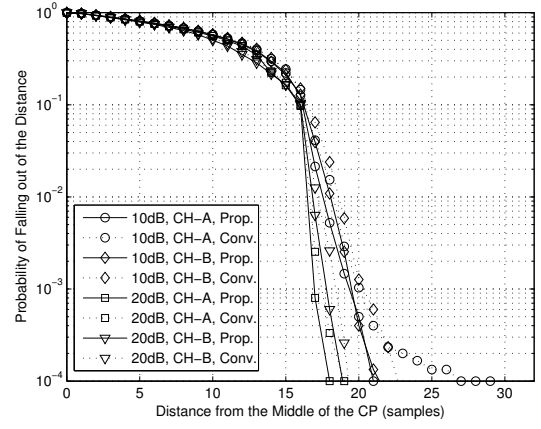
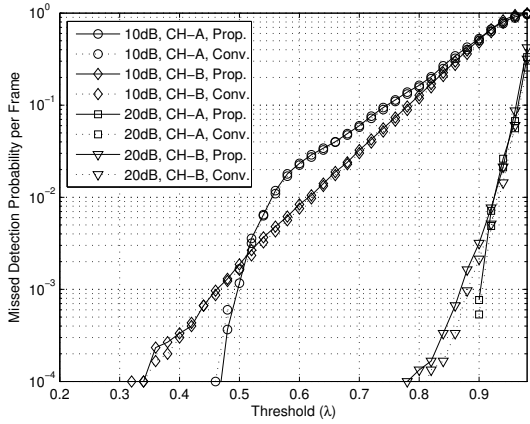
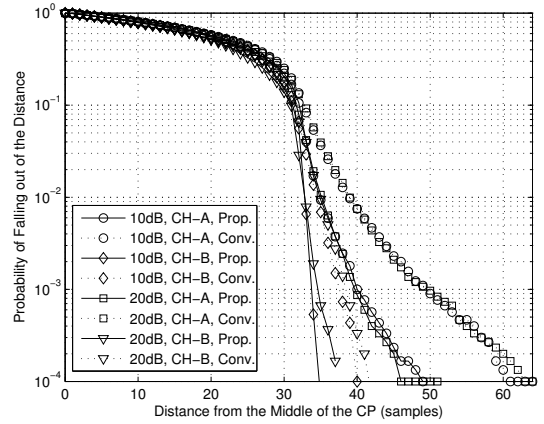
(a) OFDM physical layer ($M_1 = 4, M_2 = 2$)(a) OFDM physical layer ($M_1 = 4, M_2 = 2$)(b) OFDMA physical layer ($L_1 = 3$)(b) OFDMA physical layer ($L_1 = 3$)

Fig. 7. Missed detection probability per frame.

Fig. 8. Histogram of timing estimation error.

coarse timing estimates falling out of certain distance from the reference point. In the OFDM and OFDMA cases, the lengths of CP are 32 and 64 samples respectively, which means that the correct estimates need to be within ± 16 and ± 32 samples from the reference point for the OFDM and OFDMA cases respectively.

Using the criterion described above, in Figure 8(a) and 8(b), we see about 90% of the estimates fall in the window of correct estimates. Very steep falling edges are observed exactly at $N_g/2$. This indicates that the probability for large timing offsets or significant ISI would decay quickly out of the window of correct estimates. It is observed that the estimates of the proposed method are distributed in a narrower region around the reference timing position than that of the conventional methods [5], [12]. This suggests superior performance of the proposed algorithm. For both proposed and conventional estimators, the coarse timing estimates are evenly distributed in the window of correct estimates, so the refined timing estimation methods [7]–[9] are needed to determine the ideal timing positions.

VI. CONCLUSIONS

A universal timing metric combining algorithm is proposed in this paper to provide robust timing estimation performance in various channel conditions. The proposed method can take advantage of multiple training symbols and work in the scenario where the training symbols consist of highly correlated but not identical segments. Our analysis shows that using more correlated segments in the training symbol reduces the false alarms but has little impact on the missed detections. The simulation results under various channel conditions confirm the robustness of the proposed method.

APPENDIX A APPROXIMATION TO $R[\hat{n}_i, d]$

From (5), we can expand $R[\hat{n}_i, d]$ as

$$R[\hat{n}_i, d] = e^{j\frac{2\pi}{N}d\epsilon_0} \left(\sum_{k=0}^{N-d-1} \hat{x}^*[\hat{n}_i + k] \hat{x}[\hat{n}_i + k + d] + \sum_{k=0}^{N-d-1} w^*[\hat{n}_i + k] w[\hat{n}_i + k + d] + \Theta(\hat{n}_i, d) \right) \quad (40)$$

where $\Theta(\hat{n}_i, d)$ is defined in (7). The second term in the bracket of (40) is the summation of products of uncorrelated noise terms, its contribution to the value of $R[\hat{n}_i, d]$ is much smaller than the other terms when the signal is not weaker than the noise. The first term in the bracket is the summation of products of signal terms, which can be expanded as

$$\begin{aligned} & \hat{x}^*[\hat{n}_i + k] \hat{x}[\hat{n}_i + k + d] \\ &= \sum_{l_1=1}^{L_h} h^*[l_1] x_i^*[k - \tau[l_1]] \sum_{l_2=1}^{L_h} h[l_2] x_i[k + d - \tau[l_2]] \\ &= \sum_{l_1=1}^{L_h} |h[l_1]|^2 x_i^*[k - \tau[l_1]] x_i[k + d - \tau[l_1]] \\ &+ \sum_{l_1=1}^{L_h} \sum_{l_2 \neq l_1} h^*[l_1] h[l_2] x_i^*[k - \tau[l_1]] x_i[k + d - \tau[l_2]]. \quad (41) \end{aligned}$$

The first summation in (41) contains the products of samples with fixed distance d , which can be evaluated as

$$\begin{aligned} x_i[k]^* x_i[k + d] &= \frac{1}{N} \sum_{m_2=1}^{N_p[i]} e^{j \frac{2\pi}{N} (\vartheta_i + (m_2-1)M_i)d} \\ &\cdot \left(|X_i[m_2]|^2 + \sum_{m_1 \neq m_2} X_i^*[m_1] X_i[m_2] e^{j \frac{2\pi}{N} (m_2-m_1)M_i k} \right). \quad (42) \end{aligned}$$

Because $X_i[\cdot]$ is a pseudo-random PSK modulated training sequence, the summation of the second term in the bracket of (42) is a summation of phase rotating terms with equal magnitude, the value is close to 0. However, with properly selected d , the first term accumulates over the summation and will dominate the value of the equation. It follows that

$$\begin{aligned} x_i[k]^* x_i[k + d] &\approx |X_i[1]|^2 \frac{1}{N} \sum_{m_2=1}^{N_p[i]} e^{j \frac{2\pi}{N} (\vartheta_i + (m_2-1)M_i)d} \\ &= |X_i[1]|^2 \frac{N_p}{N} \rho_i(d) \phi_i(d) \quad (43) \end{aligned}$$

where $\rho_i(d)$ and $\phi_i(d)$ are defined in (8), and (9) respectively, and due to the PSK modulation, $|X_i[m_2]|^2 = |X_i[1]|^2$. This indicates that the correlation between the samples is high when their distance is close to a multiple of (N/M_i) , and it decays quickly as the distance to the multiple of (N/M_i) increases. We know the samples whose distance is $(d - \tau[l_2] + \tau[l_1])$ where $l_1 \neq l_2$ are weakly correlated, the summation of their products weighted by zero-mean uncorrelated channel gains must be small. Hence, we neglect the second summation in (41) and replace the first one with (43),

$$\hat{x}^*[\hat{n}_i + k] \hat{x}[\hat{n}_i + k + d] \approx |X_i[1]|^2 \frac{N_p}{N} \rho_i(d) \phi_i(d) \sum_{l_1=1}^{L_h} |h[l_1]|^2. \quad (44)$$

Substitute the summation of signal products in (40) with (44), drop the summation of uncorrelated noise products, and use the definition of σ_i^2 in (4), the approximation to $R[\hat{n}_i, d]$ is attained and shown in (6).

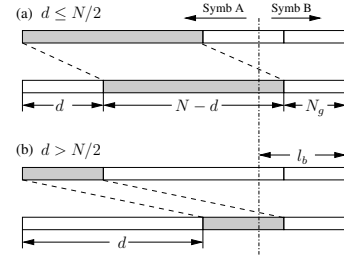


Fig. 9. Diagram of the component timing metric in the unequal power case.

APPENDIX B STATISTICAL PROPERTIES OF THE COMPONENT TIMING METRIC AT INCORRECT TIMING POSITIONS

We derive the statistical properties of the component timing metric in an AWGN channel. Following [16], we approximate the received samples at incorrect timing positions as independent complex-valued zero-mean Gaussian random variables. As pointed out in [17], the samples are correlated when there are unused subcarriers in the OFDM symbols, however, the correlation is negligible and the number of unused subcarriers is small, which is usually the case in practical OFDM systems. For instance, in the IEEE 802.16 (WiMAX) standard, the unused subcarriers (guard bands) occupy about 16% of the total spectrum.

The samples in the correlation window, i.e., from sample \bar{n}_i to $(\bar{n}_i + N - 1)$, can belong to two OFDM symbols of different power levels. Assume the boundary of the two symbols is at sample $(\bar{n}_i + (N + N_g - l_b))$. From Figure 9, we can see that the number of samples belonging to the latter OFDM symbol is given by $l_B = \max(0, l_b - N_g)$, and that of the former symbol is $l_A = (N - \max(0, l_b - N_g))$. Denote the variance of the samples of the former symbol as σ_A^2 , and that of the latter as $\eta \cdot \sigma_A^2$. It is worth mentioning that substantial power fluctuation within one symbol period violates our assumptions and leads to certain performance degradation. This effect is analyzed in Section V with simulation results.

The denominator of the component timing metric defined by (12) can be expanded as

$$R[\bar{n}_i, 0] = \sum_{k=0}^{l_A-1} |r[\bar{n}_i + k]|^2 + \sum_{k=l_A}^{N-1} |r[\bar{n}_i + k]|^2 = \chi_A + \chi_B. \quad (45)$$

where χ_A and χ_B are the summations of the squared magnitude of the samples in the former and latter symbols respectively, so they follow a Chi-square distribution with $(2l_A)$ and $(2l_B)$ degrees of freedom scaled by $\sigma_A^2/2$ and $\eta\sigma_A^2/2$ respectively. When l_A is sufficiently large, χ_A can be further approximated by a Gaussian random variable whose mean and variance are given by

$$E\{\chi_A\} = \sum_{k=0}^{l_A-1} E\{|r[\bar{n}_i + k]|^2\} = l_A \sigma_A^2, \quad (46)$$

and

$$\text{Var}\{\chi_A\} = E\{\chi_A^2\} - (E\{\chi_A\})^2$$

$$\begin{aligned}
&= \sum_{k_1=0}^{l_A-1} \sum_{k_2=0}^{l_A-1} E \{ |r[\bar{n}_i + k_1]|^2 |r[\bar{n}_i + k_2]|^2 \} - (l_A \sigma_A^2)^2 \\
&= 3 \cdot (2l_A) \left(\frac{\sigma_A^2}{2} \right)^2 + 2l_A(2l_A - 1) \left(\frac{\sigma_A^2}{2} \right)^2 - (l_A \sigma_A^2)^2 \\
&= l_A \sigma_A^4. \tag{47}
\end{aligned}$$

This suggests that the mean of χ_A equals its standard deviation multiplied by $\sqrt{l_A}$. When l_A is large, the deviation of χ_A from its mean value is small. Similarly, χ_B can also be approximated by its mean when l_B is large. It follows that

$$R[\bar{n}_i, 0] \approx E \{ \chi_A \} + E \{ \chi_B \} = (l_A + \eta l_B) \sigma_A^2. \tag{48}$$

If not both l_A and l_B are large, since $(l_A + l_B = N)$, at most one of them can be small. Without loss of generality, we assume that l_A is small. If η is large, χ_B dominates the value of $R[\bar{n}_i, 0]$, then (48) still holds. However, when η is much smaller than l_A/l_B , χ_A dominates the value of $R[\bar{n}_i, 0]$, and (48) can be violated. When this happens, we can show that the value of the component timing metric is proportional to $\sqrt{\eta}$, which must be very small and unlikely to cause any false alarms. This means that (48) is a good enough approximation, and we can write

$$\begin{aligned}
T_c[\bar{n}_i, d] &\approx \frac{N}{N-d} \frac{1}{\rho_i(d)} \frac{|R[\bar{n}_i, d]|}{E \{ |R[\bar{n}_i, 0]| \}} \\
&= \frac{N}{N-d} \frac{1}{\rho_i(d)} \frac{|R[\bar{n}_i, d]|}{(l_A + \eta l_B) \sigma_A^2}. \tag{49}
\end{aligned}$$

$|R[\bar{n}_i, d]|$ is the magnitude of the summation of a large number of zero-mean uncorrelated complex values, so it follows Rayleigh distribution. $T_c[\bar{n}_i, d]$ equals $|R[\bar{n}_i, d]|$ multiplied by a scaling factor, so approximately follows Rayleigh distribution as well. The statistical property of $T_c[\bar{n}_i, d]$ is determined by the second moment given by

$$\begin{aligned}
E \{ T_c^2[\bar{n}_i, d] \} &= \frac{1}{N + N_g} \sum_{l_b=0}^{N+N_g-1} E \{ T_c^2[\bar{n}_i, d] | l_b \} \\
&\approx \frac{1}{N + N_g} \int_0^{N+N_g} E \{ T_c^2[\bar{n}_i, d] | l_b \} dl_b \\
&\approx \frac{1}{N + N_g} \cdot \frac{N^2}{(N-d)^2} \cdot \frac{1}{\rho_i^2(d)} \\
&\quad \cdot \int_0^{N+N_g} \frac{E \{ |R[\bar{n}_i, d]|^2 | l_b \}}{((N + (\eta - 1) \max(0, l_b - N_g))^2 \sigma_A^4)} dl_b. \tag{50}
\end{aligned}$$

For a given l_b , we can write

$$\begin{aligned}
E \{ |R[\bar{n}_i, d]|^2 | l_b \} &= E \left\{ \sum_{n_1=\bar{n}_i}^{\bar{n}_i+N-d-1} |r^*[n_1]r[n_1+d]|^2 | l_b \right\} \\
&+ E \left\{ \sum_{n_1=\bar{n}_i}^{\bar{n}_i+N-d-1} \sum_{n_2 \neq n_1} r[n_1]r^*[n_2]r^*[n_1+d]r[n_2+d] | l_b \right\} \\
&= \sum_{n_1=\bar{n}_i}^{\bar{n}_i+N-d-1} E \{ |r[n_1]|^2 | l_b \} E \{ |r[n_1+d]|^2 | l_b \} \tag{51}
\end{aligned}$$

where the last equality follows the assumption on the samples' independent zero-mean Gaussian distribution. For each individual sample, l_b determines whether it belongs to the former

or latter OFDM symbol, where $E \{ |r[n_1]|^2 | l_b \}$ equals σ_A^2 and $\eta \sigma_A^2$ respectively. Define l_{AA} , l_{AB} , l_{BB} as the numbers of terms in the summation of (51) that are the products of samples both from the former symbol, one from the former one from the latter, and both from the latter symbol, respectively. Then, (51) can be simplified to

$$E \{ |R[\bar{n}_i, d]|^2 | l_b \} = (l_{AA} + \eta l_{AB} + \eta^2 l_{BB}) \sigma_A^4. \tag{52}$$

However, l_{AA} , l_{AB} , l_{BB} change with l_b differently in various scenarios. When $d \leq N/2$,

$$E \{ |R[\bar{n}_i, d]|^2 | l_b \} = \sigma_A^4 \begin{cases} (N-d), & l_b \in [0, N_g); \\ (N-d + N_g - l_b) + \eta(l_b - N_g), & l_b \in [N_g, N_g + d); \\ (N-d + N_g - l_b) + \eta d + \eta^2(l_b - d - N_g), & l_b \in [N_g + d, N_g + N - d); \\ \eta(N + N_g - l_b) + \eta^2(l_b - N_g - d), & l_b \in [N_g + N - d, N_g + N). \end{cases} \tag{53}$$

When $d > (N/2)$,

$$E \{ |R[\bar{n}_i, d]|^2 | l_b \} = \sigma_A^4 \begin{cases} (N-d), & l_b \in [0, N_g); \\ (N-d + N_g - l_b) + \eta(l_b - N_g), & l_b \in [N_g, N_g + N - d); \\ \eta(N-d), & l_b \in [N_g + N - d, N_g + d); \\ \eta(N + N_g - l_b) + \eta^2(l_b - N_g - d), & l_b \in [N_g + d, N_g + N). \end{cases} \tag{54}$$

Substitute the expectation in the integral of (50) with (53) or (54), and after some algebraic manipulation, we obtain

$$\begin{aligned}
E \{ T_c^2[\bar{n}_i, d] \} &\approx \frac{1}{N + N_g} \cdot \frac{1}{\rho_i^2(d)} \cdot \frac{N^2}{(N-d)^2} \\
&\quad \cdot \left(\frac{(N-d)N_g}{N^2} - \frac{N-d}{N} + g(\eta) \right) \tag{55}
\end{aligned}$$

where $g(\eta) \triangleq \log \left(\frac{N\eta}{(N-d)+\eta d} \right) + \frac{1}{\eta-1} \log \left(\frac{\eta(\eta(N-d)+d)}{(N-d)+\eta d} \right)$. Equation (55) holds for both ($d \leq N/2$) and ($d > N/2$) scenarios. It is easy to compute $g(\eta) = 2(1-d/N)$ as $\eta \rightarrow 1$, and $g(\eta) = \log(N/d)$ as $\eta \rightarrow 0$ or $+\infty$. Numerical results show that $g(\eta)$ is bounded by these limits and only fluctuates within a small range for all $d \geq N/8$. Considering the fact that η is more likely to fluctuate around 1, it will not introduce much error to approximate $g(\eta)$ with $g(1)$ in (55), and $E \{ T_c^2[\bar{n}_i, d] \}$ is approximately equal to $(\rho_i^2(d)(N-d))^{-1}$.

APPENDIX C

FALSE ALARM PROBABILITY OF THE COMBINED TIMING METRIC

We index all the component timing metrics from 1 to K . Suppose the k^{th} re-indexed timing metric corresponds to the m^{th} component timing metric of training symbol i , we define $b_k \triangleq \omega_{i,m}^2 \sigma_{i,m}^2$, and $\bar{b}_n \triangleq \sum_{k=1}^n b_k$. We follow the independent Gaussian distribution assumption about the samples

made in Appendix B, and can show that the component timing metrics are uncorrelated to each other at incorrect timing positions. Define

$$q_k(\lambda) \triangleq P\left(\sum_{i=1}^k T_c[\bar{n}, d_i] > \lambda\right), \quad (56)$$

which can be recursively evaluated by

$$q_1(\lambda) = 1 - \int_0^\lambda f(u_1|b_1)du_1 = e^{-\lambda^2/(2b_1)}, \quad (57)$$

$$\begin{aligned} q_{k+1}(\lambda) &= \int_0^{+\infty} P\left(\sum_{i=1}^k T_c[\bar{n}, d_i] > (\lambda - u_{k+1})\right) \\ &\quad \cdot f(u_{k+1}|b_{k+1}) du_{k+1} \\ &= \int_0^\lambda q_k(\lambda - u_{k+1}) f(u_{k+1}|b_{k+1}) du_{k+1}. \end{aligned} \quad (58)$$

Assume

$$q_k(\lambda) \approx A_k \lambda^{k-1} e^{-\lambda^2/(2\bar{b}_k)} \quad (59)$$

where

$$A_k \triangleq (\sqrt{2\pi})^{k-1} (\tilde{b}_k)^{\frac{1}{2}-k} \prod_{i=1}^k \sqrt{b_i}. \quad (60)$$

When $k = 1$, the right hand side of (59) reduces to that of (57), so (59) holds. For $k \geq 1$, assume (59) holds for q_k . In the following, we show $q_{k+1}(\lambda)$ also satisfies (59) using the recursive relationship (58).

$$\begin{aligned} &q_{k+1}(\lambda) \\ &\approx \int_0^\lambda A_k (\lambda - u)^{k-1} e^{-(\lambda-u)^2/(2\bar{b}_k)} \frac{u}{b_{k+1}} e^{-u^2/(2b_{k+1}^2)} du \\ &= \frac{A_k}{b_{k+1}} e^{-\lambda^2/(2\bar{b}_{k+1})} \int_0^\lambda u (\lambda - u)^{k-1} e^{-\frac{\left(u - \frac{b_{k+1}\lambda}{b_{k+1}}\right)^2}{2\frac{b_{k+1}\bar{b}_k}{b_{k+1}}}} du \\ &\approx \frac{A_k}{b_{k+1}} e^{-\lambda^2/(2\bar{b}_{k+1})} \lambda^k \left(\frac{b_k}{b_{k+1}}\right)^{k-1} \int_{-\infty}^{+\infty} e^{-\frac{\left(u - \frac{b_{k+1}\lambda}{b_{k+1}}\right)^2}{2\frac{b_{k+1}\bar{b}_k}{b_{k+1}}}} du \\ &= A_{k+1} \lambda^k e^{-\lambda^2/(2\bar{b}_{k+1})} \end{aligned} \quad (61)$$

where the first approximation follows the assumption about $q_k(\lambda)$, the second approximation follows the fact that the exponential term approximates 0 very quickly out of the small region around $u = \frac{b_{k+1}}{b_{k+1}}\lambda$. Therefore, (59) holds for all k . Combining it with (56), (17) is obtained. The derivation indicates that the approximation is accurate for large λ values.

APPENDIX D

THE MEAN AND VARIANCE OF $Z_A[\hat{n}_1]$ AND $Z_C[\hat{n}_1]$

Because Case A can be seen as a special case of Case C, the mean and variance of $Z_A[\hat{n}_1]$ can be obtained by simplifying those of $Z_C[\hat{n}_1]$ with an extra condition ($\rho_{1,k} = 1$). The mean of $Z_C[\hat{n}_1]$ can be directly computed from (36) as

$$E\{Z_C[\hat{n}_1]\} = N\sigma_1^2 - \lambda N(\sigma_1^2 + \sigma_w^2). \quad (62)$$

The variance of $Z_C[\hat{n}_1]$ is given by

$$\begin{aligned} Var\{Z_C[\hat{n}_1]\} &= \lambda^2 E\{\tilde{R}[\hat{n}_i, 0]^2\} + \left(\frac{2}{\sum_{k=1}^{K_1} \rho_1^2(d_{1,k})}\right)^2 \\ &\quad \cdot \sum_{k_1=1}^{K_1} \sum_{k_2=1}^{K_1} |\rho_1(d_{1,k_1})\rho_1(d_{1,k_2})| E\{\tilde{R}[\hat{n}_1, d_{1,k_1}]\tilde{R}[\hat{n}_1, d_{1,k_2}]\} \\ &\quad - 2\lambda \left(\frac{2}{\sum_{k=1}^{K_1} \rho_1^2(d_{1,k})}\right) \sum_{k=1}^{K_1} |\rho_1(d_{1,k_1})| \\ &\quad \cdot E\{\tilde{R}[\hat{n}_1, d_{1,k_1}]\tilde{R}[\hat{n}_1, 0]\} \end{aligned} \quad (63)$$

where we define $\gamma_i(d)$ as the sign of $\rho_i(d)$ and

$$\tilde{R}[\hat{n}_i, 0] = \tilde{R}[\hat{n}_i, 0] - E\{\tilde{R}[\hat{n}_i, 0]\} \approx \Theta(\hat{n}_i, 0), \quad (64)$$

$$\begin{aligned} \tilde{R}[\hat{n}_i, d] &= |\tilde{R}[\hat{n}_i, d]| - E\{|\tilde{R}[\hat{n}_i, d]|\} \\ &\approx \gamma_i(d) \Re\{\phi_i^*(d)\Theta(\hat{n}_i, d)\}. \end{aligned} \quad (65)$$

For all $d_1 \leq d_2$, we can show that

$$\begin{aligned} E\{\Theta^*(\hat{n}_i, d_1)\Theta(\hat{n}_i, d_2)\} &= 2\sigma_i^2 \sigma_w^2 \phi_i(d_2 - d_1) \rho_i(d_2 - d_1) \\ &\quad \cdot (N - d_2) \end{aligned} \quad (66)$$

$$\begin{aligned} E\{\Theta(\hat{n}_i, d_1)\Theta(\hat{n}_i, d_2)\} &= 2\sigma_i^2 \sigma_w^2 \phi_i(d_2 + d_1) \rho_i(d_2 + d_1) \\ &\quad \cdot \max(N - d_1 - d_2, 0). \end{aligned} \quad (67)$$

It immediately follows that

$$E\{\tilde{R}[\hat{n}_i, 0]^2\} \approx 2N\sigma_i^2 \sigma_w^2 \quad (68)$$

$$\begin{aligned} E\{\tilde{R}[\hat{n}_i, d]\tilde{R}[\hat{n}_i, 0]\} &\approx (N - d) |\rho_i(d)| \sigma_i^2 \\ &\quad \cdot (N\sigma_i^2 + \sigma_w^2) + 2\sigma_w^2 \end{aligned} \quad (69)$$

$$\begin{aligned} E\{\tilde{R}[\hat{n}_i, d_1]\tilde{R}[\hat{n}_i, d_2]\} &\approx \gamma_i(d_1)\gamma_i(d_2) ((N - d_2) \\ &\quad \cdot \rho_i(d_2 - d_1) + \rho_i(d_2 + d_1) \\ &\quad \cdot \max(N - d_2 - d_1, 0)). \end{aligned} \quad (70)$$

Thus, $Var\{Z_C[\hat{n}_1]\}$ can be obtained by substituting (68), (69) and (70) into (63), and the result is shown in (38). Let all $\rho_i(d) = 1$ in (38), we can simplify the expression for the variance of $Z_A[\hat{n}_1]$ to that in (26).

APPENDIX E

THE MEAN AND VARIANCE OF $Z_B[\hat{n}_1]$

The mean of $Z_B[\hat{n}_1]$ can be directly evaluated by

$$E\{Z_B[\hat{n}_1]\} = N^2\sigma_1^2(\sigma_1^2 + \sigma_w^2) - \lambda N^2(\sigma_1^2 + \sigma_w^2)^2. \quad (71)$$

The second moment of $Z_B[\hat{n}_1]$ can be expanded to

$$\begin{aligned} E\{Z_B[\hat{n}_1]^2\} &= \lambda^2 E\{R[\hat{n}_1, 0]^2\} E\{R[\hat{n}_2, 0]^2\} \\ &\quad + E\left\{(|R_{B,1}[\hat{n}_1]|R[\hat{n}_2, 0] + |R_{B,2}[\hat{n}_2]|R[\hat{n}_1, 0])^2\right\} \\ &\quad - \lambda E\{|R_{B,1}[\hat{n}_1]|R[\hat{n}_1, 0]\} E\{|R_{B,2}[\hat{n}_2]|^2\} \\ &\quad - \lambda E\{|R_{B,2}[\hat{n}_2]|R[\hat{n}_2, 0]\} E\{|R_{B,1}[\hat{n}_1]|^2\}. \end{aligned} \quad (72)$$

According to the definition of $R_{B,i}[\hat{n}_i]$, we can compute

$$\begin{aligned} &E\{R_{B,i}[\hat{n}_i]R[\hat{n}_i, 0]\} \\ &= N\sigma_i^2 (N(\sigma_i^2 + \sigma_w^2) + 2\sigma_w^2) \frac{M_i - 1}{M_1 + M_2 - 2}. \end{aligned} \quad (73)$$

Also,

$$\begin{aligned}
& E \{ |R_{B,i}[\hat{n}_i]|^2 \} \\
&= \left(\frac{2}{M_1 + M_2 - 2} \right)^2 \sum_{k_1=1}^{M_i-1} \sum_{k_2=1}^{M_i-1} E \{ |R[\hat{n}_i, d_{i,k_1}] R[\hat{n}_i, d_{i,k_2}]| \} \\
&= N\sigma_i^2 (N\sigma_i^2 + 2\sigma_w^2) \left(\frac{M_i - 1}{M_1 + M_2 - 2} \right)^2. \quad (74)
\end{aligned}$$

Thus, ignoring the higher order noise terms, we can approximate the products of expectations as

$$\begin{aligned}
& E \{ (R_{B,1}[\hat{n}_1]R[\hat{n}_2, 0] + R_{B,2}[\hat{n}_2]R[\hat{n}_1, 0])^2 \} \\
&\approx N^4\sigma_1^6(\sigma_1^2 + 2\sigma_w^2) + 4N^3\sigma_1^6\sigma_w^2 \quad (75)
\end{aligned}$$

$$\begin{aligned}
& E \{ R[\hat{n}_1, 0]^2 \} E \{ R[\hat{n}_2, 0]^2 \} \\
&\approx N^4\sigma_1^6(\sigma_1^2 + 4\sigma_w^2) + 4N^3\sigma_1^6\sigma_w^2 \quad (76)
\end{aligned}$$

$$\begin{aligned}
& E \{ R_{B,1}[\hat{n}_1]R[\hat{n}_1, 0] \} E \{ R^2[\hat{n}_2, 0] \} \\
&\approx (N^4\sigma_1^6(\sigma_1^2 + 3\sigma_w^2) + 4N^3\sigma_1^6\sigma_w^2) \frac{M_1 - 1}{M_1 + M_2 - 2} \quad (77)
\end{aligned}$$

$$\begin{aligned}
& E \{ R_{B,2}[\hat{n}_2]R[\hat{n}_2, 0] \} E \{ R^2[\hat{n}_1, 0] \} \\
&\approx (N^4\sigma_1^6(\sigma_1^2 + 3\sigma_w^2) + 4N^3\sigma_1^6\sigma_w^2) \frac{M_2 - 1}{M_1 + M_2 - 2}. \quad (78)
\end{aligned}$$

Combine them with (72), then minus the square of the mean given by (71), (32) is attained.

REFERENCES

- [1] T. M. Schmidl and D. C. Cox, "Robust frequency and timing synchronization for OFDM," *IEEE Transactions on Communications*, vol. 45, pp. 1613–1621, Dec. 1997.
- [2] A. J. Coulson, "Maximum likelihood synchronization for OFDM using a pilot symbol: algorithm," *IEEE Journal on Selected Areas in Communications*, vol. 19, pp. 2486–2494, Dec. 2001.
- [3] —, "Maximum likelihood synchronization for OFDM using a pilot symbol: analysis," *IEEE Journal on Selected Areas in Communications*, vol. 19, pp. 2495–2503, Dec. 2001.
- [4] H. Minn, V. K. Bhargava, and K. B. Letaief, "A robust timing and frequency synchronization for OFDM systems," *IEEE Transactions on Wireless Communications*, vol. 2, Jul. 2003.
- [5] K. Shi and E. Serpedin, "Coarse frame and carrier synchronization of OFDM systems: a new metric and comparison," *IEEE Transactions on Wireless Communications*, vol. 3, Jul. 2004.
- [6] Y. Li, J. L. J. Cimini, and N. R. Sollenberger, "Robust channel estimation for OFDM systems with rapid dispersive fading channels," *IEEE Transactions on Communications*, vol. 46, pp. 902–915, Jul. 1998.
- [7] E. G. Larsson, G. Liu, J. Li, and G. B. Giannakis, "Joint symbol timing and channel estimation for OFDM-based WLANs," *IEEE Communication Letters*, vol. 5, pp. 325–327, Aug. 2001.
- [8] R. A. Pacheco, O. Üreten, D. Hatzinakos, and N. Serinken, "Bayesian frame synchronization using periodic preamble for OFDM-based WLANs," *IEEE Signal Processing Letters*, vol. 12, pp. 524–527, Jul. 2005.
- [9] H. Minn, V. K. Bhargava, and K. B. Letaief, "A combined timing and frequency synchronization and channel estimation for OFDM," *IEEE Transactions on Communications*, vol. 54, pp. 416–422, Mar. 2006.
- [10] IEEE, *Par 11: Wireless LAN medium access control (MAC) and physical layer (PHY) specifications: high-speed physical layer in the 5 GHz band*. IEEE-SA Standards Board, 2003.
- [11] —, *IEEE Standard for local and metropolitan area networks, part 16: air interface for fixed mobile broadband wireless access systems, amendment 2: physical and medium access control layers for combined fixed and mobile operation in licensed bands and corrigendum 1*. <http://ieeexplore.ieee.org/servlet/opac?punumber=10676>, 2006.
- [12] T. Bhatt, V. Sundaramurthy, J. Zhang, and D. McCain, "Initial synchronization for 802.16e downlink," in *Proc. the Fortieth Asilomar Conference on signals, systems and computers (ACSSC)*, Oct. 2006.
- [13] IEEE LAN/MAN Standards Committee, "Channel models for fixed wireless applications," *Document IEEE 802.16.3c-01/29r4*, 2003.
- [14] ITU-R M.1225, "Guidelines for evaluation of radio transmission technologies for IMT-2000," *Recommendation ITU-R M 1225*, 1997.
- [15] W. C. Jakes Jr. (Editor), *Microwave mobile communications*. J. Wiley & Sons, 1974.
- [16] Jan-Jaap van de Beek, M. Sandell, and P. O. Börjesson, "ML estimation of time and frequency offset in OFDM systems," *IEEE Transactions on Signal Processing*, vol. 45, pp. 1800–1805, Jul. 1997.
- [17] S. H. Müller-Weinfurter, "On the optimality of metrics for coarse frame synchronization in OFDM: a comparison," in *Proc. the Ninth IEEE International Symposium on Personal, Indoor and Mobile Radio Communications*, vol. 2, Sep. 1998, pp. 533 – 537.



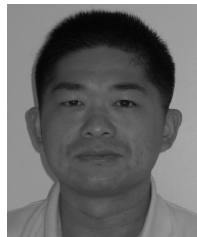
Ming (Matt) Ruan

Ming (Matt) Ruan received the B.Eng and M.Eng degrees from Shanghai Jiaotong University, Shanghai, China, in 1998 and 2001, respectively. Then he joined Lucent Bell Labs China as a member of technical staff. In 2005 he immigrated to Australia and became a PhD candidate in the Australian National University with the support of an Australian Postgraduate Award (APA) and a supplemental scholarship from the National ICT Australia (NICTA). Since 2008 he has been working at NICTA as a research engineer. His current research interests include synchronization technologies, statistical signal processing, and iterative receiver design.



Mark C. Reed

Mark C. Reed has worked in industry and research positions for the last 18 years with positions in the U.S.A., Switzerland, and Australia. He pioneered the area of iterative receiver design as part of his doctoral studies and was part of a team that designed and developed a world first Satellite-UMTS Modem for the European Space Agency. He also completed further work on 3G Basestation design as technical lead in the highly successful European Commission project, ASILUM, which investigated and validated advanced signal processing schemes for link improvement in UMTS. Since April 2003 Dr Reed is employed as a Principal Researcher at National ICT Australia (NICTA), and is an Adjunct Associate Professor at the Australian National University, Canberra, Australia, where he is involved in research, education, and commercialization, within the wireless signal processing program. He has over 45 international journal and conference papers, was previously an Associate Editor for the *IEEE Transactions on Vehicular Technology*, and has been listed as inventor on eight patent applications.



Zhenning Shi

Zhenning Shi received the BS degree in Electronics Engineering from Tsinghua University, China, in 1998, and the PhD degree in Electrical and Computer Engineering from the University of Utah, US, in 2003. From 2002 to 2004, he was a post-doctoral fellow at the Electrical and Computer Engineering Department, the University of Utah. In 2004, he joined NICTA and has been with the Canberra Research Lab since then. He is also an adjunct research fellow at Australian National University (ANU), where he is involved in the joint education and research program in wireless communications. Dr. Zhenning Shi's primary research interests include multiuser detection, iterative receivers, channel estimation, equalization and synchronization in CDMA, OFDMA and LTE. He has published over 50 technical papers and filed 4 patent applications in these areas.